ACSNANO
www.acsnano.org
ARTICLE

Conjugated Polymer Blend Microspheres for Efficient, Long-Range Light Energy Transfer

Soh Kushida,[†] Daniel Braam,[‡] Thang Duy Dao,[§,∥] Hitoshi Saito,[†] Kosuke Shibasaki,[†] Satoshi Ishii,[§,∥] Tadaaki Nagao,[§,∥] Akinori Saeki,[⊥] Junpei Kuwabara,[†,#] Takaki Kanbara,[†,#,¶] Masashi Kijima,[†,#] Axel Lorke,[‡] and Yohei Yamamoto*[,†,#,¶]

[†]Division of Materials Science, Faculty of Pure and Applied Sciences, University of Tsukuba, 1-1-1 Tennodai, Tsukuba, Ibaraki 305-8571, Japan

[‡]Faculty of Physics and CENIDE, University of Duisburg-Essen, Lotharstrasse 1, Duisburg D-47048, Germany

[§]International Center for Materials Nanoarchitectonics (WPI-MANA), National Institute for Materials Science (NIMS), 1-1 Namiki, Tsukuba, Ibaraki 305-0044, Japan

[∥]CREST, Japan Science and Technology Agency (JST), 4-1-8 Honcho, Kawaguchi, Saitama 332-0012, Japan

[⊥]Department of Applied Chemistry, Graduate School of Engineering, Osaka University, 2-1 Yamadaoka, Suita, Osaka 565-0871, Japan

[#]Tsukuba Research Center for Interdisciplinary Materials Science (TIMS), Faculty of Pure and Applied Sciences, University of Tsukuba, 1-1-1 Tennodai, Tsukuba, Ibaraki 305-8573, Japan

[¶]Center for Integrated Research in Fundamental Science and Technology (CiRfSE), University of Tsukuba, 1-1-1 Tennodai, Tsukuba, Ibaraki 305-8571, Japan

S *Supporting Information*

ABSTRACT: **Highly luminescent π-conjugated polymeric microspheres were fabricated through self-assembly of energy-donating and energy-accepting polymers and their blends. To avoid macroscopic phase separation, the nucleation time and growth rate of each polymer in the solution were properly adjusted. Photoluminescence (PL) studies showed that efficient donor-to-acceptor energy transfer takes place inside the microspheres, revealing that two polymers are well-blended in the microspheres. Focused laser irradiation of a single microsphere excites whispering gallery modes (WGMs), where PL generated inside the sphere is confined and resonates. The wavelengths of the PL lines are finely tuned by changing the blending ratio, accompanying the systematic yellow-to-red color change. Furthermore, when several microspheres are coupled linearly, the confined PL propagates the microspheres through the contact point, and a cascade-like process converts the PL color while maintaining the WGM characteristics. The self-assembly strategy for the formation of polymeric nano- to microstructures with highly miscible polymer blends will be advantageous for optoelectronic and photonic device applications.**

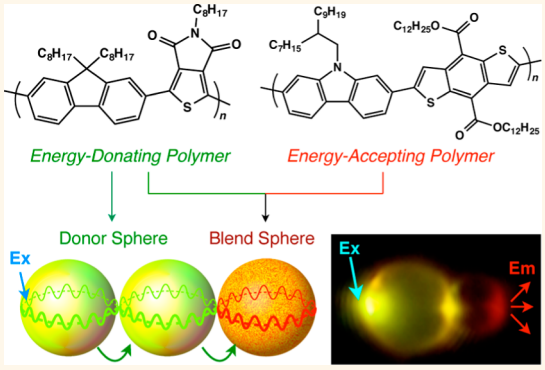

KEYWORDS: *conjugated polymer, polymer blend, microsphere, energy transfer, whispering gallery mode*

Control of the mixing state and morphology of conjugated polymers plays an important role in polymer optoelectronic devices. For example, in polymer solar cells, an appropriate nanophase segregation of electron-donating polymers and electron-accepting small molecules leads to efficient photoinduced charge separation and subsequent charge carrier conduction, due to the large-area heterointerfaces and bicontinuous charge-transporting pathways.[1−3] Likewise, in polymer light-emitting devices, fluorophores are properly placed in the charge-transporting layers, and for efficient color conversion by Förster resonant energy transfer (FRET), energy-donating and energy-accepting molecules have to be located within a 10 nm distance.[4−6] In general, different polymers are immiscible with one another because of the small mixing entropy and tend to form macroscopic phase separation.[7−11] Such separation gives rise to lowering the efficiency of the device performance. Therefore, the combination of polymers with small molecules is often employed: electron-donating polymers with fullerene derivatives for

Received: March 27, 2016
Accepted: May 2, 2016
Published: May 2, 2016

DOI: 10.1021/acsnano.6b02100
ACS Nano 2016, 10, 5543−5549

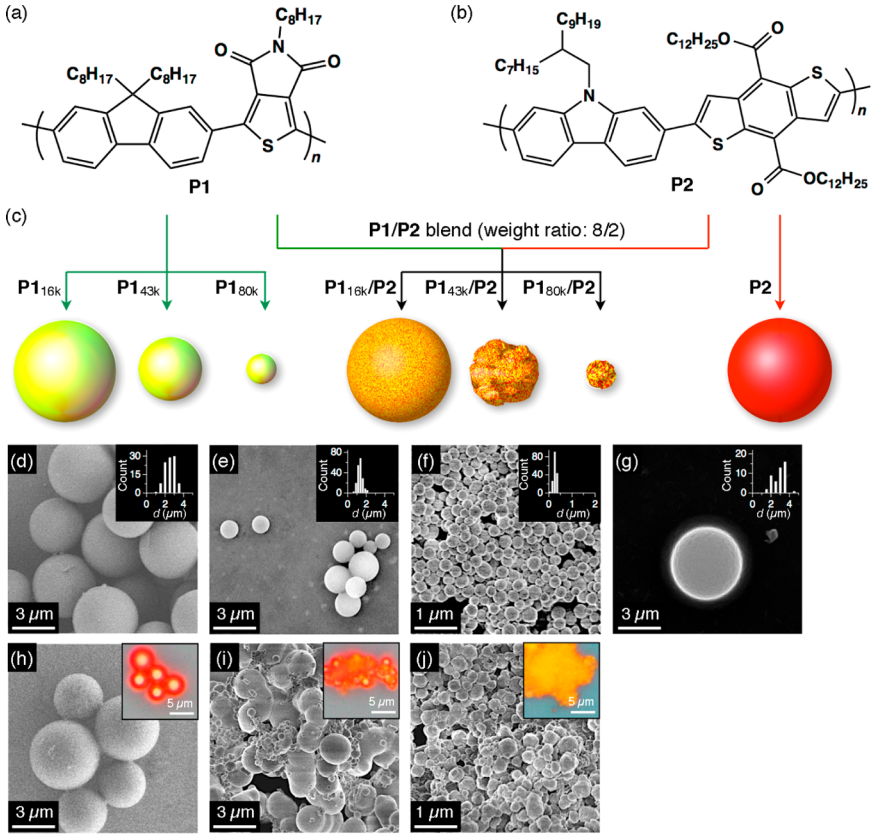

Figure 1. (a,b) Molecular structures of π-conjugated alternating copolymers P1 and P2. (c) Schematic representations of the assembling structures from P1, P1/P2 blends (f = 0.2), and P2. (d–g) SEM micrographs of self-assembled precipitates from $P1_{16k}$ (d), $P1_{43k}$ (e), $P1_{80k}$ (f), and P2 (g). Inset shows histogram of d. (h–j) SEM micrographs of self-assembled precipitates from blends of $P1_{16k}$/P2 (h), $P1_{43k}$/P2 (i), and $P1_{80k}$/P2 (j) with f = 0.2. Inset shows optical micrographs of the precipitates.

organic solar cells[1−3] and charge-transporting polymers with fluorescent small molecules in light-emitting diodes.[6]

In this article, we report the self-assembly of highly fluorescent energy-donating and energy-accepting polymers from the mixture of a solution. Recently, we developed a technique to fabricate well-defined microspheres by self-assembly of π-conjugated polymers.[12,13] The key factors for the formation of spherical structures are the low crystallinity of the polymer main chain and a slow diffusion of the polar nonsolvent into the solution of polymers. We found that these microspheres act as both fluorophore and resonator; the fluorescent microcavities exhibit resonant photoluminescence (PL) from whispering gallery modes (WGMs) upon photoexcitation.[14,15] The polymers used in the present research, when assembled alone (homotropic assembly), form well-defined spheres with sub- to several micrometer diameters depending on their molecular weight. On the other hand, when assembled from their mixed solution (heterotropic assembly), the polymers with mismatched molecular weights are immiscible with one another, only giving irregular aggregates. However, when molecular weights are identical and the nucleation time and growth rate of the polymers match well under the vapor diffusion condition, well-defined microspheres are formed exclusively. PL experiments clearly show that an efficient FRET occurs inside the microspheres, indicating that these polymers are highly miscible with one another in the microspheres. Upon focused laser excitation, a single microsphere exhibits WGM PL as a result of the confinement of PL inside the microsphere. The PL color shifts systematically, depending on the mixing ratio of the polymers. Furthermore, by connecting the microspheres, long-range PL propagation and subsequent color conversion are achieved. The self-assembly strategy for obtaining highly miscible polymer blends within nano- to microstructures will be advantageous for the use of electronically and optically active polymers to optoelectronic device applications.

RESULTS AND DISCUSSION

Self-Assembly of Energy-Donating and Energy-Accepting Polymers and Their Blends. An alternating copolymer **P1** (Figure 1a), composed of 9,9-dioctylfluorene and 5-octylthieno[3,4-*c*]pyrrole-4,6-dione with a number-average molecular weight (M_n) of 16.2, 43.0, and 79.6 kg mol^{-1} ($\mathbf{P1}_{16k}$, $\mathbf{P1}_{43k}$, and $\mathbf{P1}_{80k}$, respectively), was synthesized according to the reported procedure.[16] Another alternating copolymer **P2** (Figure 1b), comprising *N*-(2-heptylundecyl)-carbazole and 4,8-bis[(dodecyl)carbonyl]benzo[1,2-*b*:4,5-*b*′]-dithiophene repeating unit and M_n = 11.0 kg mol^{-1}, was newly synthesized (see the Supporting Information). In the thin film form, **P2** exhibits maximum photoabsorption (λ_{abs}) and PL (λ_{em}) wavelengths of 533 and 622 nm, respectively (Table S1). Because the PL band of **P1** (λ_{em} = 540 nm) overlaps considerably with the photoabsorption band of **P2** (Figure S1a), photoinduced **P1**-to-**P2** energy transfer possibly takes place. Indeed, PL spectra of thin films of $\mathbf{P1}_{16k}$ and **P2**, prepared from a solution of their blend by spin-casting, showed that as little as 1−5 wt % of **P2** resulted in a pronounced red shift of λ_{em} (Figures 2a and S1b). The PL was not quenched

DOI: 10.1021/acsnano.6b02100
ACS Nano 2016, 10, 5543−5549

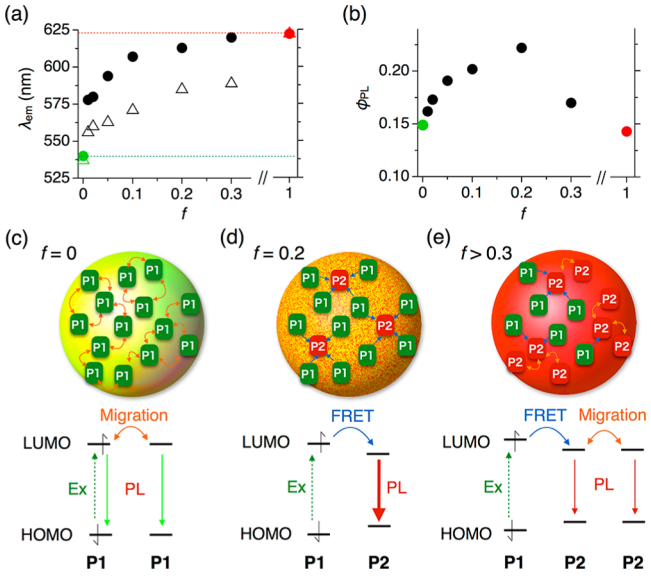

Figure 2. (a) Plots of the maximum wavelength of PL (λ_{em}) for films of the microspheres (circles) and those formed by spin-casting from $CHCl_3$ solution (triangles) *versus f*. Broken lines show λ_{em} of spin-cast thin films of $\mathbf{P1}_{16k}$ (green, λ_{em} = 537 nm) and **P2** (red, λ_{em} = 622 nm); λ_{ex} = 450 nm. (b) Plot of ϕ_{PL} for films of the microspheres *versus f*. (c–e) Schematic representations of energy migration and energy transfer inside a single microsphere with f = 0 (c), f = 0.2 (d), and f > 0.3 (e).

but was instead enhanced by the addition of **P2** (Figure S1c and Table S2), indicating that photoinduced **P1**-to-**P2** energy transfer, rather than electron transfer, takes place efficiently.

Self-assembly of the polymers was conducted by a vapor diffusion method (see Methods).[12,13] Scanning electron microscopy (SEM) shows that **P1** and **P2** exclusively form well-defined microspheres (Figure 1d–g). With increasing M_n, the diameter (d) of the spheres decreases; the average diameters d_{av} for $\mathbf{P1}_{16k}$, $\mathbf{P1}_{43k}$, and $\mathbf{P1}_{80k}$ are 2.79, 1.31, and 0.26 μm, respectively. Polymers with high M_n tend to have low solubility, resulting in a rapid precipitation and thus yielding small spheres.[12,13] The d_{av} value of **P2** is 3.10 μm.

Heterotropic assembly of **P1**/**P2** was investigated with the weight fraction of **P2** (f) set at 0.2. SEM of the resultant precipitates showed that the $\mathbf{P1}_{16k}$/**P2** blend produced well-defined microspheres with d_{av} of 3.35 μm (Figure 1h). In contrast, blends from $\mathbf{P1}_{43k}$/**P2** and $\mathbf{P1}_{80k}$/**P2** only resulted in irregular aggregates (Figure 1i,j). Because $\mathbf{P1}_{16k}$ and **P2** have nearly identical M_n, and their homotropic assemblies produce spheres with similar d values (~3 μm, Figure 1d,g), nucleation of both polymers starts at the same time, and growth rate is also similar. On the other hand, due to the larger M_n, $\mathbf{P1}_{43k}$ and $\mathbf{P1}_{80k}$ have lower solubility in $CHCl_3$ compared with $\mathbf{P1}_{16k}$, resulting in a rapid precipitation that inhibits formation of microspheres by blending with **P2**.

With increasing M_n of **P1**, PL spectra of the blended precipitate showed a small red shift (Figure S1d). Fluorescence microscopy (FM) of the precipitate from the $\mathbf{P1}_{80k}$/**P2** blend displayed a yellowish-orange PL color (Figure 1j, inset), which was different from the reddish PL from microspheres of the $\mathbf{P1}_{16k}$/**P2** blend (Figure 1h, inset). The spectroscopic and microscopic results indicate that $\mathbf{P1}_{16k}$ and **P2** are homogeneously blended in the microspheres, whereas $\mathbf{P1}_{43k}$ and $\mathbf{P1}_{80k}$ are less miscible with **P2**.

Blends of $\mathbf{P1}_{16k}$/**P2** with different ratios (f = 0.01, 0.02, 0.05, 0.1, 0.2, and 0.3) all formed microspheres with d_{av} values in the range of 1.8–4.6 μm (Figure S2 and Table S2). The surface morphology of the microspheres with small blending ratios (f = 0.02 and 0.05) appears relatively disordered (Figure S2c,d) compared to those with higher f. PL spectra showed that λ_{em} values are strongly red-shifted upon blending with only a small amount of **P2** (Figures 2a and S1e and Table S2), and the FM images also showed a clear color change from yellow to reddish orange (Figure S2, inset). The PL spectrum of the thin film of the blended microspheres with f = 0.3 closely resembles that of the microspheres of **P2** (Figures 2a and S1e). The spectroscopic changes indicate that $\mathbf{P1}_{16k}$-to-**P2** FRET takes place efficiently inside the spheres. In general, polymer blends tend to undergo phase separation when condensed from a solution due to their small mixing entropies.[7–11] In the present

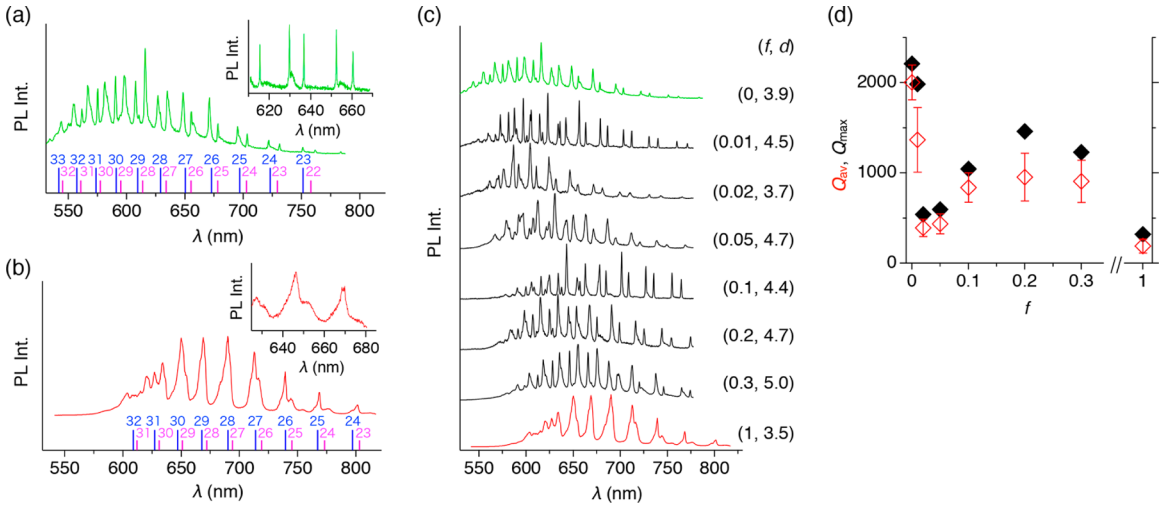

Figure 3. (a,b) μ-PL spectra of D (a) and A (b). Grating: 300 grooves mm^{-1}. The lines and numbers indicate simulated WGM peak wavelengths and indices with TE (pink) and TM (blue) modes. Inset shows μ-PL spectra of D and A with high resolution. Grating: 1200 grooves mm^{-1}. (c) μ-PL spectra of D (green), A (red), and B (black). Grating: 300 grooves mm^{-1}. The f and d values are denoted on the left side. (d) Plots of Q_{av} (red) and Q_{max} (black) *versus f*.

DOI: 10.1021/acsnano.6b02100
ACS Nano 2016, 10, 5543–5549

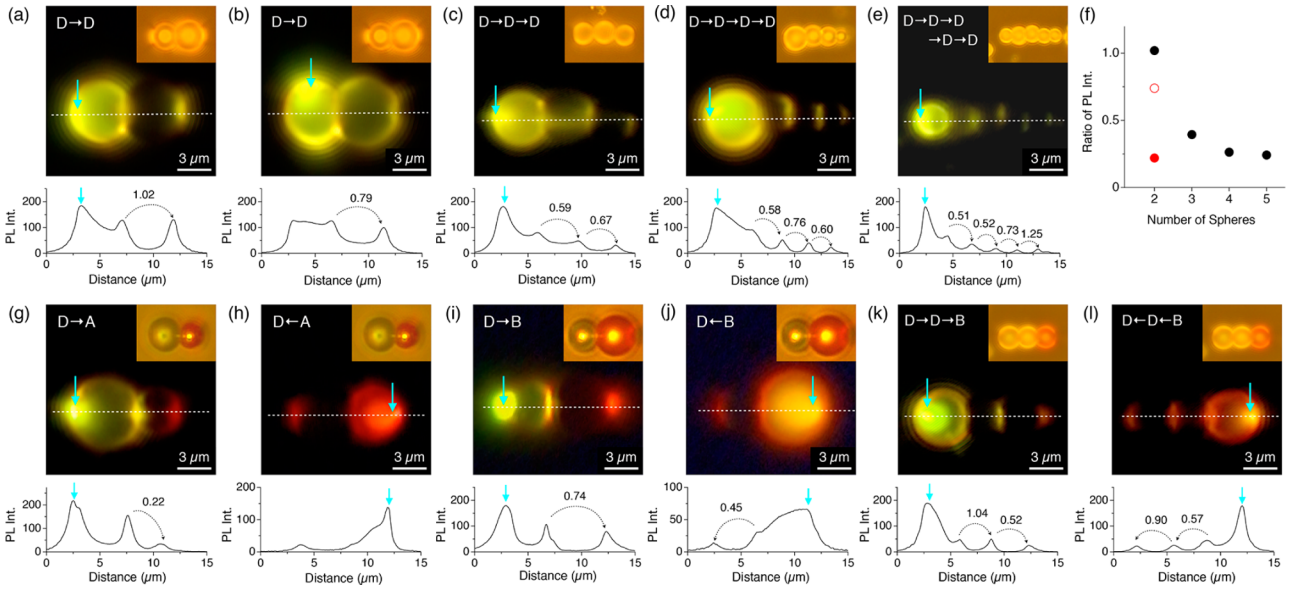

Figure 4. Fluorescent micrographs of coupled two Ds (a,b), three Ds (c), four Ds (d), and five Ds (e), D−A (g,h), D−B (i,j), and D−D−B (k,l), upon focused laser excitation (blue arrow). The graphs at the bottom of each micrograph show cross-section PL intensity profiles at the broken white lines in each micrograph. Insets show optical micrographs. Images of (a) and (b), (g) and (h), (i) and (j), and (k) and (l) are the same area with different excitation position. (f) Plots of the PL intensity ratio *versus* the number of the spheres, calculated from the cross-section profiles. Black, coupled Ds; red filled, coupled D−A; red open, coupled D−B.

study, the nucleation timing and growth rate of two polymers was properly adjusted, leading to the formation of microspheres with highly miscible polymer blends.

The PL quantum yield (ϕ_{PL}) of $\mathbf{P1}_{16k}$/**P2** blend microspheres was largely enhanced compared to those made from homotropic assembly of $\mathbf{P1}_{16k}$ or **P2** (Figure 2b and Table S2). With increasing f, ϕ_{PL} first increases to a maximum of 0.222 at f = 0.2 and then decreases. In the homotropic microspheres from $\mathbf{P1}_{16k}$ and **P2**, $\mathbf{P1}_{16k}$-to-$\mathbf{P1}_{16k}$ and **P2**-to-**P2** interpolymer energy migration takes place (Figure 2c). This exciton migration results in a decrease of ϕ_{PL} (0.149 and 0.143 for microspheres with f = 0 and 1, respectively) due to the concentration quenching.[9] Meanwhile, heterotropic microspheres, produced by blending a small amount of **P2**, undergo $\mathbf{P1}_{16k}$-to-**P2** FRET and subsequent exciton localization at **P2**, which is referred to as the dilution effect, sensitization *via* FRET that suppresses the quenching (Figure 2d).[9] A further increase in f to 0.3 resulted in a decrease in ϕ_{PL} to 0.170 (Figure 2b and Table S2) because of the subsequent **P2**-to-**P2** energy migration after $\mathbf{P1}_{16k}$-to-**P2** FRET (Figure 2e). For dye-doped polymer microcavities, several examples have so far been reported on FRET inside a microsphere.[17,18] In comparison with the dye-doped systems, our system utilizing blends of conjugated polymers is outstanding in the following points: (1) high photoabsorption efficiency, (2) high donor-to-acceptor energy transfer efficiency, and (3) enhanced ϕ_{PL} upon blending two polymers.

The enhanced ϕ_{PL}, resulting from blending $\mathbf{P1}_{16k}$ and **P2**, is also confirmed from the change of the PL lifetimes (Figure S3 and Table S3). As f increased from 0 to 0.1, the PL decay at 520 nm (PL mainly from $\mathbf{P1}_{16k}$) occurred more rapidly because of the $\mathbf{P1}_{16k}$-to-**P2** energy transfer (Figure S3a). Meanwhile, the PL at 670 nm (PL mainly from **P2**) decayed much more slowly as f increased from 0 to 0.3 (Figure S3b). This increase of the PL lifetime (τ) indicates that the nonradiative decay is certainly suppressed by blending $\mathbf{P1}_{16k}$ and **P2**. The average lifetime (τ_{av}) at 670 nm (Figure S3b, inset) follows the same trend of ϕ_{PL} (Figure 2b) as f is changed.

Resonant PL from a Single Microsphere and Intrasphere FRET. Using a μ-PL experimental setup (see Methods and Figure S4), PL spectra from a single microsphere of $\mathbf{P1}_{16k}$, **P2**, and their blends (hereafter, these microspheres are abbreviated as **D**, **A**, and **B**, respectively) were measured. Figure 3a,b shows PL spectra of single **D** and **A** with a d of 3.9 and 3.5 μm, respectively, upon focused laser irradiation (λ_{ex} = 470 nm) at the perimeter of the microsphere. Both **D** and **A** exhibit sharp and periodic PL lines within the wavelength region of their intrinsic PL. These characteristic PL lines are attributed to WGM, where PL generated inside the sphere is confined *via* total internal reflection at the polymer/air interface. The resonance occurs when the wavelength of the light is an integer multiple of the circumference of the microspheres.[14,15,19−24]

The observed PL lines correspond well to the simulated transverse electric (TE, pink) and transverse magnetic (TM, blue) modes (Figure 3a,b) using eqs S1 and S2[25] and the average refractive indices (η) of 1.8 and 2.0 for $\mathbf{P1}_{16k}$ and **P2**, respectively, evaluated by spectroscopic ellipsometry (Figure S5). The Q-factors of the WGM PL lines, defined as the wavelength divided by the full width at half-maximum of a cavity resonance, are as large as 2200 for **D**. By contrast, the highest Q-factor (Q_{max}) of **A** is only 320. The difference between these values is attributed to the surface structure: **D** possesses a smooth surface (Figure 1d), whereas the surface of **A** is relatively rough (Figure 1g), which results in a scattering loss at the surface.[26]

The PL spectra of **B** with different f values exhibit WGM PL peaks (Figure 3c). Similar to the case with the PL shift for thin films of the microspheres, WGM PL from a single sphere shifts to the longer wavelength region as f increases (Figure 3c). The wavelength region of the WGM PL of **B** with f = 0.3 nearly coincides with that of **A**, indicating that PL is generated from the **P2** species *via* $\mathbf{P1}_{16k}$-to-**P2** FRET inside **B**. Figure 3d shows plots of Q_{max} and the average Q-factor (Q_{av}) evaluated from the high-resolution PL spectra (Figure S6). A small weight fraction

DOI: 10.1021/acsnano.6b02100
ACS Nano 2016, 10, 5543−5549

of **P2** (f = 0.02 and 0.05) results in an abrupt decrease in the Q-factors, possibly caused by the scattering at the disordered surfaces of the microspheres (Figure S2c,d).[26] A further increase in f enhances Q-factors and displays a local maximum at f = 0.2 (Q_{max} = 1460), which is 4.5-fold larger in comparison with that of **A** (Q_{max} = 320). The high values of both ϕ_{PL} (Figure 2b) and Q-factor (Figure 3d) for **B** at f = 0.2 indicate that heterotropic assembly occurs successfully at this ratio, giving the microspheres with homogeneously blended $\mathbf{P1}_{16k}$ and **P2** a highly smooth surface morphology.

Long-Range Energy Transfer through Coupled Microspheres. Laser excitation at the perimeter of **D** results in bright PL at both the excited position and its diametrically opposed position because all confined light passes through the position opposed to the excited spot (Figure S7a). Accordingly, two peaks appear in the cross-section profile of the PL intensity of **D** (Figure S7a, bottom); the broad peak near the excitation spot involves both direct PL (not confined) and WGM PL (confined), whereas the sharp peak at the right side of the sphere is mainly derived from WGM. Similarly, **A** also shows two peaks (Figure S7b). However, the intensity at the opposed position to the excitation spot is rather weak because of the weaker light confinement of **A** compared with that of **D**. By contrast, **B** (hereafter, **B** indicates microspheres with f = 0.2) shows a much sharper peak compared to that of **A** due to the stronger confinement due to the higher sphericity (Figure S7c).

When two **D**s are coupled and the left side of one **D** is photoexcited, the confined PL propagates to the other **D** through the contact point, resulting in a yellow PL at the opposite side (Figure 4a). According to the cross-section PL intensity profile, the ratio of the PL intensity for the **D** → **D** propagation reaches near unity (~1.02 in Figure 4a, bottom). Even when the excitation spot is changed to a position approximately 90° from the contact point, PL propagates directionally to the adjacent **D**, and the ratio of the propagation retains its high value (~0.79, Figure 4b). Furthermore, in case of linearly connected 3−5 **D**s, propagation of the confined PL is observed (Figure 4c−e),[27] and the ratios of the propagation between adjacent **D**s are in all cases higher than 0.5 (Figure 4c−e, bottom), yet the total ratio of the PL propagation decreased monotonically as the number of **D** increased (Figure 4f, black). However, it is quite contrastive when two **D**s were separated and one **D** was photoexcited, where PL generated from one **D** hardly propagates to the other **D** because of the lack of bridged **D** that mediates directional PL propagation (Figure S7d).

Next, intersphere PL propagation with coupled **D** and **A** spheres is studied. Upon photoexcitation of **D**, a yellow PL is observed from **D**, and red PL is observed from **A** at the location opposite the contact point (Figure 4g). In contrast, when **A** is photoexcited, red PL is observed at the excitation, contact, and opposite points (Figure 4h). The PL behavior in Figure 4g is referred to as cascading energy transfer: A 470 nm blue laser light excites **D**, which generates yellow PL. The confined yellow PL travels directionally across the contact point and is reabsorbed by **P2**, and then, the red PL is generated in **A**. The possibility that the blue excitation light leaks to **A** and directly excites **P2** can be ruled out from the results of the excitation of **A**; if the blue excitation light leaks into the other microsphere, the PL from **D** in Figure 4h would be yellow. The leakage of the excitation light is actually negligible because both **P1** and **P2** possess high absorptivity at 470 nm.

According to the PL intensity profiles, the ratio of the **D** → **A** propagation is only 0.22, possibly because of the low confinement efficiency of **A** (Figure 4f, red filled, and 4g, bottom). Moreover, the **A** → **D** propagation is less efficient (Figure 4h, bottom) because η of **P2** is larger than that of $\mathbf{P1}_{16k}$ at the wavelength region above 530 nm (Figure S5). However, the efficiencies of the intersphere energy transfer are greatly improved by replacing **A** with **B** as the counterpart of **D**. Upon photoexcitation of **D**, red PL is observed from **B** in addition to the yellow PL from **D** (Figure 4i). The **D** → **B** propagation ratio reaches 0.74 (Figure 4f, red open, and 4i, bottom). Such a high propagation ratio is attributed a 1.5-fold higher ϕ_{PL} of **B** as well as the smoother surface morphology compared with **A**. Similarly, the **B** → **D** propagation efficiency is significantly enhanced (0.45, Figure 4j, bottom) compared with the **A** → **D** propagation (Figure 4h, bottom).

The WGM characteristic is preserved after propagation of the PL across the spheres. Experimentally, for the coupled **D**−**B**, the perimeters of **D** and **B** are photoexcited (denoted as $\mathbf{D}_{ex}$ and $\mathbf{B}_{ex}$, respectively), and PL from **D** and **B** are detected (denoted as $\mathbf{D}_{em}$ and $\mathbf{B}_{em}$, respectively; see the schematic illustrations in Figure S8). The PL spectra I ($\mathbf{D}_{ex}$−$\mathbf{D}_{em}$) and IV ($\mathbf{B}_{ex}$−$\mathbf{B}_{em}$) in Figure S8, in which the excitation and detection spots coincide, involve WGMs of **D** and **B**, respectively. Interestingly, the PL spectra II ($\mathbf{D}_{ex}$−$\mathbf{B}_{em}$) and III ($\mathbf{B}_{ex}$−$\mathbf{D}_{em}$) exhibit WGMs, which are the spectroscopic fingerprints of both **B** and **D**. In the PL spectrum II, a WGM from **D** still remains, but those from **B** appear, which results from the reabsorption of the propagated light below the absorption edge of **P2** (~570 nm) and subsequent PL by the **P2** species that is confined in **B**. By contrast, the spectrum III is more complex. The PL comes from **P2** in **B**, but it involves WGMs originating from both **B** and **D**. In addition, new WGMs appear that are not observed in either spectrum I or IV (Figure S8, green dots), which most likely is attributed to mode coupling of **B** and **D**.[28,29] For comparison, when the coupled **D**−**B** is separated by using a micromanipulation technique, WGM characteristics of each microsphere are enhanced (Figure S9), indicating a decrease of the cavity properties by contacting microspheres.

We further demonstrate the WGM-mediated long-range energy transfer by using three spheres, **D**, **D**, and **B**, which are lined up in this order (Figure 4k,l). When the left **D** is photoexcited, yellow PL propagates to the central **D** and is converted to red PL at the right **B** (Figure 4k). Conversely, when the right **B** is photoexcited, red PL propagates to the central and left **D** without any color change (Figure 4l). Such cascading energy transfer by WGM-mediated light propagation across several microspheres is intriguing, taking advantage of **B** with well-blended polymers that possesses superior ϕ_{PL} and Q-factor values compared to those of **A**.

CONCLUSIONS

We demonstrate homotropic and heterotropic assemblies of highly fluorescent π-conjugated polymers that form well-defined microspheres. The heterotropic assembly results in highly miscible polymer blend microspheres only when two polymers have similar molecular weights, and thus the precipitation time is nearly identical. PL from a single microsphere exhibits WGMs involving sharp and periodic PL lines with Q-factors as high as 2200. The WGM PL with a successive yellow-to-red color change occurs by changing the blend ratio, in which efficient intrasphere donor-to-acceptor FRET takes place. Furthermore, intersphere light propagation

DOI: 10.1021/acsnano.6b02100
ACS Nano 2016, 10, 5543−5549

and cascading color conversion are observed through a WGM-mediated energy transfer process. The color conversion occurs more efficiently when the polymer blend microspheres are used as the energy-accepting microspheres. The long-range and efficient energy transfer using conjugated polymer microspheres will be beneficial for application to soft optoelectronic and photonic devices.

METHODS

Preparation of Microspheres. Typically, a 5 mL vial containing a $CHCl_3$ solution of **P1**, **P2**, or their blends with a total concentration and amount of 0.5 mg mL^{-1} and 2 mL, respectively, was placed in a 50 mL vial containing 5 mL of nonsolvent, such as MeOH and MeCN. The outside vial was capped and then allowed to stand for 3 days at 25 °C. The vapor of the nonsolvent was slowly diffused into the solution, resulting in a precipitation of the polymers through the supersaturated state.

μ-PL Measurements. μ-PL measurements were carried out using a μ-PL measurement system (Figure S4). An optical microscope was used with a long-distance 100× objective (NA = 0.8) to identify suitable particles and determine their diameters (d). For measurements, a WITec μ-PL system was used with a model Alpha 300S microscope combined with a Princeton Instruments model Acton SP2300 monochromator (grating: 300 or 1200 grooves mm^{-1}) and an Andor iDus model DU-401A BR-DD-352 CCD camera cooled to −60 °C. The edge of a single sphere was photoexcited at 25 °C under ambient conditions by a diode pulsed laser (a PicoQuant model LDH-D-C-470B with a PDL 828 "Sepia II" driver) with the wavelength, power, integration time, frequency, pulse duration, and spot size of 470 nm, 1.5 μW, 0.1 s, 2.5 MHz, 70 ps, and ∼0.5 μm, respectively.[14] For the preparation of the coupled **D**s and coupled **D**−**B**, a suspension of **D** or a mixture of the suspensions of **D** and **B** was deposited by spin-casting (1500 rpm for 40 s and then 3000 rpm for 20 s) on a quartz substrate and air-dried. For the preparation of the coupled **D**−**A**, a suspension of **A** was drop-cast and dried under a reduced pressure, and then a suspension of **D** was deposited by spin-casting (1500 rpm for 40 s and then 3000 rpm for 20 s) onto the substrate and air-dried.

μ-PL Measurements at Different Excitation and Detection Positions. The microspheres were photoexcited by a 405 nm Linos Nano-405-80 laser, and the light was collected within a confocal setup by a 50× objective with NA = 0.5 and detected by a 500 mm Acton SpectraPro 2500i spectrometer with a liquid-nitrogen-cooled CCD camera at −120 °C and a 150 mm^{-1} grating.[13] Spot size, laser power, and integration time were 0.5 μm, 0.5 μW, and 1 s, respectively. To separate the detection spot from the excitation, the collimator optics of the excitation laser beam was tilted with respect to the optical axis of the detection path.

ASSOCIATED CONTENT

Supporting Information

The Supporting Information is available free of charge on the ACS Publications website at DOI: 10.1021/acsnano.6b02100.

Materials and measurements, synthesis, characterization, simulation, Figures S1−S9, and Tables S1−S3 (PDF)

AUTHOR INFORMATION

Corresponding Author

*E-mail: yamamoto@ims.tsukuba.ac.jp.

Notes

The authors declare no competing financial interest.

ACKNOWLEDGMENTS

The authors acknowledge Prof. Masaki Yamamura and Prof. Tatsuya Nabeshima at the University of Tsukuba for their assistance with fluorescence quantum yield measurements. This work was partly supported by a Grant-in-Aid for Young Scientists A (25708020), Exploratory Research (15K13812), Scientific Research on Innovative Areas "π-System Figuration" (15H00986) and "Artificial Photosynthesis" (15H00860) from JSPS/MEXT Japan, Industrial Technology Research Grant Program from NEDO Japan, Asahi Glass Foundation, and the University of Tsukuba−DAAD partnership program.

REFERENCES

(1) Peet, J.; Senatore, M. L.; Heeger, A. J.; Bazan, G. C. The Role of Processing in the Fabrication and Optimization of Plastic Solar Cells. *Adv. Mater.* **2009**, *21*, 1521−1527.

(2) Kim, F. S.; Ren, G.; Jenekhe, S. A. One-Dimensional Nanostructures of π-Conjugated Molecular Systems: Assembly, Properties, and Applications from Photovoltaics, Sensors, and Nanophotonics to Nanoelectronics. *Chem. Mater.* **2011**, *23*, 682−732.

(3) Beaujuge, P. M.; Fréchet, J. M. J. Molecular Design and Ordering Effects in π-Functional Materials for Transistor and Solar Cell Applications. *J. Am. Chem. Soc.* **2011**, *133*, 20009−20029.

(4) Friend, R. H.; Gymer, R. W.; Holmes, A. B.; Burroughes, J. H.; Marks, R. N.; Taliani, C.; Bradley, D. D. C.; Dos Santos, D. A.; Brédas, J. L.; Lögdlund, M.; Salaneck, W. R. Electroluminescence in Conjugated Polymers. *Nature* **1999**, *397*, 121−128.

(5) Huang, J.; Li, G.; Wu, E.; Xu, Q.; Yang, Y. Achieving High-Efficiency Polymer White-Light-Emitting Devices. *Adv. Mater.* **2006**, *18*, 114−117.

(6) Niu, X.; Ma, L.; Yao, B.; Ding, J.; Tu, G.; Xie, Z.; Wang, L. White Polymeric Light-Emitting Diodes with High Color Rendering Index. *Appl. Phys. Lett.* **2006**, *89*, 213508.

(7) Bates, F. S. Polymer-Polymer Phase Behavior. *Science* **1991**, *251*, 898−905.

(8) Kietzke, T.; Neher, D.; Landfester, K.; Montenegro, R.; Güntner, R.; Scherf, U. Novel Approaches to Polymer Blends Based on Polymer Nanoparticles. *Nat. Mater.* **2003**, *2*, 408−412.

(9) Pan, C.; Sugiyasu, K.; Takeuchi, M. Blending Conjugated Polymers without Phase Separation for Fluorescent Colour Tuning of Polymeric Materials through FRET. *Chem. Commun.* **2014**, *50*, 11814−11817.

(10) Zhou, K.; Liu, J.; Li, M.; Yu, X.; Xing, R.; Han, Y. Phase Diagram of Conjugated Polymer Blend P3HT/PF12TBT and the Morphology-Dependent Photovoltaic Performance. *J. Phys. Chem. C* **2015**, *119*, 1729−1736.

(11) Uemura, T.; Kaseda, T.; Sasaki, Y.; Inukai, M.; Toriyama, T.; Takahara, A.; Jinnai, H.; Kitagaewa, S. Mixing of Immiscible Polymers Using Nanoporous Coordination Templates. *Nat. Commun.* **2015**, *6*, 7473.

(12) Adachi, T.; Tong, L.; Kuwabara, J.; Kanbara, T.; Saeki, A.; Seki, S.; Yamamoto, Y. Spherical Assemblies from π-Conjugated Alternating Copolymers: Toward Optoelectronic Colloidal Crystals. *J. Am. Chem. Soc.* **2013**, *135*, 870−876.

(13) Tong, L.; Kushida, S.; Kuwabara, J.; Kanbara, T.; Ishii, N.; Saeki, A.; Seki, S.; Furumi, S.; Yamamoto, Y. Tetramethylbithiophene in π-Conjugated Alternating Copolymers as an Effective Structural Component for the Formation of Spherical Assemblies. *Polym. Chem.* **2014**, *5*, 3583−3587.

(14) Tabata, K.; Braam, D.; Kushida, S.; Tong, L.; Kuwabara, J.; Kanbara, T.; Beckel, A.; Lorke, A.; Yamamoto, Y. Self-Assembled Conjugated Polymer Spheres as Fluorescent Microresonators. *Sci. Rep.* **2014**, *4*, 5902.

(15) Kushida, S.; Braam, D.; Pan, C.; Dao, T. D.; Tabata, K.; Sugiyasu, K.; Takeuchi, M.; Ishii, S.; Nagao, T.; Lorke, A.; Yamamoto, Y. Whispering Gallery Resonance from Self-Assembled Microspheres of Highly Fluorescent Isolated Conjugated Polymers. *Macromolecules* **2015**, *48*, 3928−3933.

(16) Saito, H.; Kuwabara, J.; Kanbara, T. Facile Synthesis of Fluorene-Based π-Conjugated Polymers *via* Sequential Bromination/Direct Arylation Polycondensation. *J. Polym. Sci., Part A: Polym. Chem.* **2015**, *53*, 2198−2201.

DOI: 10.1021/acsnano.6b02100
ACS Nano 2016, 10, 5543−5549

(17) Folan, L. M.; Arnold, S.; Druger, S. D. Enhanced Energy Transfer within a Microparticle. *Chem. Phys. Lett.* **1985**, *118*, 322−327.
(18) Fujiwara, H.; Sasaki, K.; Masuhara, H. Enhancement of Förster Energy Transfer within a Microspherical Cavity. *ChemPhysChem* **2005**, *6*, 2410−2416.
(19) Chen, R.; Ta, V. D.; Sun, H. D. Single Mode Lasing from Hybrid Hemispherical Microresonators. *Sci. Rep.* **2012**, *2*, 244.
(20) Ta, V. D.; Chen, R.; Sun, H. D. Tuning Whispering Gallery Mode Lasing from Self-Assembled Polymer Droplets. *Sci. Rep.* **2013**, *3*, 1362.
(21) Wang, X.; Li, H.; Wu, Y.; Xu, Z.; Fu, H. Tunable Morphology of the Self-Assembled Organic Microcrystals for the Efficient Laser Optical Resonator by Molecular Modulation. *J. Am. Chem. Soc.* **2014**, *136*, 16602−16608.
(22) Wei, C.; Liu, S.-Y.; Zou, C.-L.; Liu, Y.; Yao, J.; Zhao, Y. S. Controlled Self-Assembly of Organic Composite Microdisks for Efficient Output Coupling of Whispering-Gallery-Mode Lasers. *J. Am. Chem. Soc.* **2015**, *137*, 62−65.
(23) Wang, X.; Liao, Q.; Li, H.; Bai, S.; Wu, Y.; Lu, X.; Hu, H.; Shi, Q.; Fu, H. Near-Infrared Lasing from Small-Molecule Organic Hemispheres. *J. Am. Chem. Soc.* **2015**, *137*, 9289−9295.
(24) Narayana, Y. S. L. V.; Venkatakrishnarao, D.; Biswas, A.; Mohiddon, M. A.; Viswanathan, N.; Chandrasekar, R. Visible−Near-Infrared Range Whispering Gallery Resonance from Photonic μ-Sphere Cavities Self-Assembled from a Blend of Polystyrene and Poly[4,7-bis(3-octylthiophene-2-yl)benzothiadiazole-co-2,6-bis-(pyrazolyl)pyridine] Coordinated to $Tb(acac)_3$. *ACS Appl. Mater. Interfaces* **2016**, *8*, 952−958.
(25) Oraevsky, A. N. Whispering-Gallery Waves. *Quantum Electron.* **2002**, *32*, 377−400.
(26) Braginsky, V. B.; Gorodetsky, M. L.; Ilchenko, V. S. Quality Factor and Nonlinear Properties of Optical Whispering-Gallery Modes. *Phys. Lett. A* **1989**, *137*, 393−397.
(27) Chen, Z.; Taflove, A.; Backman, V. Highly Efficient Optical Coupling and Transport Phenomena in Chains of Dielectric Microspheres. *Opt. Lett.* **2006**, *31*, 389−391.
(28) Mukaiyama, T.; Takeda, K.; Miyazaki, H.; Jimba, Y.; Kuwata-Gonokami, M. Tight-Binding Photonic Molecule Modes of Resonant Bispheres. *Phys. Rev. Lett.* **1999**, *82*, 4623−4626.
(29) Kanaev, A. V.; Astratov, V. N.; Cai, W. Optical Coupling at a Distance Between Detuned Spherical Cavities. *Appl. Phys. Lett.* **2006**, *88*, 111111.

DOI: 10.1021/acsnano.6b02100
ACS Nano 2016, 10, 5543−5549